Approximating snow surface temperature from standard temperature and humidity data: New possibilities for snow model and remote sensing evaluation

Mark S. Raleigh,[1] Christopher C. Landry,[2] Masaki Hayashi,[3] William L. Quinton,[4] and Jessica D. Lundquist[5]

Received 11 April 2013; revised 28 October 2013; accepted 31 October 2013; published 9 December 2013.

[1] Snow surface temperature (T_s) is important to the snowmelt energy balance and land-atmosphere interactions, but in situ measurements are rare, thus limiting evaluation of remote sensing data sets and distributed models. Here we test simple T_s approximations with standard height (2–4 m) air temperature (T_a), wet-bulb temperature (T_w), and dew point temperature (T_d), which are more readily available than T_s. We used hourly measurements from seven sites to understand which T_s approximation is most robust and how T_s representation varies with climate, time of day, and atmospheric conditions (stability and radiation). T_d approximated T_s with the lowest overall bias, ranging from −2.3 to +2.6°C across sites and from −2.8 to 1.5°C across the diurnal cycle. Prior studies have approximated T_s with T_a, which was the least robust predictor of T_s at all sites. Approximation of T_s with T_d was most reliable at night, at sites with infrequent clear sky conditions, and at windier sites (i.e., more frequent turbulent instability). We illustrate how mean daily T_d can help detect surface energy balance bias in a physically based snowmelt model. The results imply that spatial T_d data sets may be useful for evaluating snow models and remote sensing products in data sparse regions, such as alpine, cold prairie, or Arctic regions. To realize this potential, more routine observations of humidity are needed. Improved understanding of T_d variations will advance understanding of T_s in space and time, providing a simple yet robust measure of snow surface feedback to the atmosphere.

Citation: Raleigh, M. S., C. C. Landry, M. Hayashi, W. L. Quinton, and J. D. Lundquist (2013), Approximating snow surface temperature from standard temperature and humidity data: New possibilities for snow model and remote sensing evaluation, *Water Resour. Res.*, *49*, 8053–8069, doi:10.1002/2013WR013958.

1. Introduction

[2] The surface temperature of snow (T_s) is a critical factor in the snow energy balance and in land-atmosphere interactions, modulating how much energy is used to warm or melt a snowpack and how much energy is returned to the atmosphere. In the literature, the term "snow surface temperature" has been used to refer to two distinct yet related variables: radiant surface temperature (i.e., the "skin" of the snowpack that emits longwave radiation to the atmosphere) and thermodynamic surface temperature (i.e., the bulk temperature of a thin layer at the snowpack surface). Radiant T_s controls outgoing longwave radiation and regulates the near-surface profiles of temperature and vapor pressure that influence sensible and latent heat transfer. Increases in thermodynamic T_s drive the growth of snow grains, reducing snow surface albedo and enhancing absorbed shortwave radiation [*Flanner and Zender*, 2006]. Thermodynamic T_s is also important for slab avalanche formation, as large diurnal temperature fluctuations in near-surface snow layers can induce kinetic metamorphism and form faceted snow grains [*Armstrong and Armstrong*, 1987; *Birkeland*, 1998; *Birkeland et al*., 1998]. When combined with a vapor gradient directed from the atmosphere to the snow surface, T_s can produce surface hoar. When buried, faceted snow grains and surface hoar can form weak layers in a snowpack [*Stössel et al*., 2010]. Finally, radiant T_s is important for winter recreation (e.g., downhill skiing and cross-country skiing races) [e.g., *Wagner and Horel*, 2011], as it has a nonlinear relationship with surface friction [*Colbeck*, 1988].

[3] Despite its importance, T_s is rarely measured at existing observational networks [*Bales et al*., 2006]. For example, in the western US, fewer than 2% of snow-measuring automatic weather stations also measure radiant T_s [*Raleigh*, 2013]. Thermodynamic T_s is typically measured by avalanche centers via manual snow pit profiles, but these measurements are generally limited in space and time (e.g.,

Additional supporting information may be found in the online version of this article.

[1]National Center for Atmospheric Research, Boulder, Colorado, USA.
[2]Center for Snow and Avalanche Studies, Silverton, Colorado, USA.
[3]Department of Geoscience, University of Calgary, Calgary, Alberta, Canada.
[4]Centre for Cold Regions and Water Science, Wilfrid Laurier University, Waterloo, Ontario, Canada.
[5]Department of Civil and Environmental Engineering, University of Washington, Seattle, Washington, USA.

Corresponding author: M. Raleigh, National Center for Atmospheric Research, 3450 Mitchell Ln., Boulder, CO 80301, USA. (raleigh@ucar.edu)

0043-1397/13/10.1002/2013WR013958

daily or weekly). Thus, T_s is often acquired with remote sensing or modeling. Satellite-based remote sensing of surface emission at infrared wavelengths has yielded T_s data sets, but atmospheric emission of longwave radiation complicates this methodology [*Duguay*, 1993], and few studies have validated remotely sensed T_s, as noted by *Dozier and Painter* [2004]. In modeling applications, T_s has been estimated with (1) empirical relationships that track hourly [*Marks et al*., 1992; *Brubaker et al*., 1996] or mean daily [*Molotch*, 2009] air temperature, (2) conceptual approaches based on air temperature that incorporate radiative cooling effects [*Marsh and Pomeroy*, 1996; *Pohl et al*., 2006], (3) longwave-based psychrometric formulations [e.g., *Ellis et al*., 2010], and (4) physically based approaches that solve for T_s in the surface energy balance using analytic [e.g., *Kondo and Yamazaki*, 1990; *Essery and Etchevers*, 2004] or iterative solutions [*Outcalt*, 1972; *Outcalt et al*., 1975; *Jordan*, 1991; *Tarboton and Luce*, 1996]. Due to the inherent scarcity of T_s observations, models generally lack validation of this important parameter. Instead, snow models are typically evaluated only against the mass balance via snow water equivalent (SWE) data [*Essery and Etchevers*, 2004], a practice which neglects the energy balance and limits process-based understanding [*Clark et al*., 2011]. Depending on model selection, uncertainty in midwinter T_s may be as large as 8–10°C [*Slater et al*., 2001; *Essery et al*., 2013], yielding up to 40 W m^{-2} of uncertainty in longwave emitted to the atmosphere, and signifying problems in the modeled surface energy balance.

[4] In contrast to the above methods for estimating T_s, *Andreas* [1986] hypothesized that the dew point temperature (T_d) of air close to the snow surface approximates T_s. The physical reason for this approximation is that snow cover is a saturated surface, such that the vapor pressure (e) of air close to the surface equals the saturation vapor pressure (e_{sat}). Air reaches saturation at T_d, and e_{sat} is a function of T_s alone; thus, T_d close to the snow surface is expected to be in equilibrium with T_s. Supporting this reasoning, *U.S. Army Corps of Engineers* [1956] notes that "The vapor pressure has a strong tendency to remain close to that of the snow surface since the snowpack is both a sink and a source for vapor pressure greater or less than that of the snow. For air over a melting snowpack, the tendency is thus toward a vapor pressure of 6.11 millibars (the saturated vapor pressure at 32°F)." While *Andreas* [1986] focused on T_d, there exists a second saturation temperature, the wet-bulb temperature (T_w) (see section 3), which is the temperature at which an air parcel becomes saturated through evaporative cooling. For an unsaturated air parcel, T_w is always greater than T_d. The relationship between T_w and T_s has seen little attention in the literature.

[5] *Andreas* [1986] first supported his hypothesis with theoretical analysis, which showed T_d is representative of T_s during periods with enhanced mixing (i.e., high wind speed) or when the near-surface vapor pressure gradient weakens (e.g., when e_{air} comes into equilibrium with $e_{sat}(T_s)$). He then demonstrated that different T_s measurements generally corresponded to T_d measurements 10 cm above the snow surface during January 1984 at a field site in Michigan. He compared T_d to both thermodynamic T_s (measured with thermistors and thermocouples 1–5 cm below the snow surface) and radiant T_s (measured with an infrared sensor). Based on his field measurements, he found that approximation of T_s with T_d was accurate to ±1°C. However, he found that T_s for all three sensors (infrared sensor, thermistors, and thermocouples) was higher than T_d during sunny periods and assumed that solar heating had biased the sensors.

[6] To date, the results of *Andreas* [1986] have seen limited application in snow hydrology research, perhaps because T_d measurements are rarely taken close to the snow surface [*Marks et al*., 1992]. Temperature sensors and hygrometers are typically installed at a standard height 2–4 m above the ground surface at a climate station, with the height above the snow surface varying as the snow depth fluctuates with accumulation, wind scour/deposition, compaction, sublimation, and melt processes. Therefore, it remains unknown how saturation temperatures at standard height relate to T_s, how these relationships vary with local conditions (i.e., boundary layer stability and radiation), and whether they approximate T_s more reliably than air temperature. There is also limited understanding of how well saturation temperatures approximate T_s in other snow climates within the cryosphere, as the relationship has only been tested over snow cover in Michigan [*Andreas*, 1986] and over polar sea ice [*Andreas et al*., 2002]. Finally, the experiment of *Andreas* [1986] was confined to a single month in midwinter, so it is unknown how this approximation varies throughout the entire cold season.

[7] The purpose of this paper is to test representations of T_s with standard height measurements across a more complete range of seasonally snow-covered environments, climates, and seasons. We seek to know how accurately T_s may be approximated with as few parameters as possible, so as to make the results applicable to remote, snow-dominant regions where meteorological observations are often scarce. Humidity measurements are found at 35% of stations in the western US [*Raleigh*, 2013], so they are comparatively more abundant than T_s observations. We specifically address three key questions: (1) How do measurements of T_s compare to standard height dry bulb (i.e., air) temperature (T_a), wet-bulb temperature (T_w), and dew point temperature (T_d)?, (2) How well does standard height T_d represent T_s climatically and diurnally?, (3) How well does T_d approximate T_s with variations in atmospheric conditions (i.e., radiation and stability)?. We address the above questions using measurements at seven sites located across North America and Europe. To illustrate the relevance of these results to model evaluation, we also compared T_d measurements with those simulated by a physically based snow model (SNTHERM) [*Jordan*, 1991] for both cases of best-available forcing data and of biased forcing data.

[8] The approximation of both radiant T_s and thermodynamic T_s are considered in this study. Radiant T_s is considered in the surface measurement analysis while thermodynamic T_s is considered in the modeling case study. The results related to radiant T_s are most applicable to remote sensing applications (see section 6). Both types of T_s are broadly relevant to snow models and the calculation of surface fluxes, as some snow models simulate radiant T_s (e.g., the Utah Energy Balance [*Tarboton and Luce*, 1996]) while other models (e.g., SNTHERM) simulate thermodynamic T_s for the top snow layer (with finite thickness).

2. Sites and Data

[9] We selected study sites in wet and dry climates that featured all surface observations required to test and compare the T_s approximations (Table 1 and Figure 1). Météo-France provided an 18 year data set from the Col de Porte site (CDP) in a subalpine maritime environment [*Morin et al*., 2012]. The United States Army Corps of Engineers Cold Regions Research and Engineering Laboratory (CRREL) provided data at a low elevation, moist continental site (South Royalton Vermont, SRV) [*Peck and Fiori*, 1992]. The IP3 (Improved Processes and Parameterizations for Prediction in Cold Regions) Research Network (http://www.usask.ca/ip3/) provided data from stations in a wet alpine environment (Opabin, OPB) [*Hood and Hayashi*, 2010] and a subarctic bog in the zone of discontinuous permafrost (Scotty Bog, BOG) [*Williams et al*., 2013]. The University of Calgary provided data from a cold grassland prairie (Spy Hill, SPY) [*Mohammed et al*., 2013]. The Center for Snow and Avalanche Studies (http://www.snowstudies.org) provided data from paired sites in a dry continental climate, including a subalpine site (Swamp Angel Study Plot, SASP) and an alpine site (Senator Beck Study Plot, SBSP). Although SASP and SBSP were located in the same climate, they provided insights into windy (SBSP) versus sheltered (SASP) locations. Mean December-January-February (DJF) temperatures at the sites ranged from −0.90 to −22°C (Table 1).

[10] The study period depended on data availability at each site, and ranged from 1 to 18 snow years (Table 1). All sites recorded 30 min or hourly measurements of air temperature, humidity, wind speed, snow depth, downwelling shortwave and longwave radiation, and either infrared-measured T_s or upwelling longwave radiation (i.e., from the downward-pointing pyrgeometer on a net radiometer). The meteorological measurements were made at a fixed height above the ground at all sites except for CDP, where operators adjusted the instrument heights weekly to maintain a consistent height above the snow surface [*Morin et al*., 2012].

[11] Air temperature measurements were made with a mechanically aspirated sensor at CDP and with naturally ventilated sensors at the remaining six sites (Table 1). Naturally ventilated temperature sensors may be subject to radiative heating errors during days with high solar radiation and low wind speeds [e.g., *Kent et al*., 1993; *Huwald et al*., 2009]. Radiative errors tend to be higher over snow surfaces than other land types because the high albedo of snow directs additional energy to the temperature sensor [*Huwald et al*., 2009]. For example, maximum radiative errors have been documented in the 6.2–10°C range in the cryosphere [*Arck and Scherer*, 2001; *Georges and Kaser*, 2002; *Huwald et al*., 2009], compared to 3.4–4.0°C in oceanic environments [*Kent et al*., 1993; *Anderson and Baumgartner*, 1998] and 1.2–2.2°C in summer grasslands [*Nakamura and Mahrt*, 2005; *Mauder et al*., 2008]. An auxiliary analysis (see supporting information 1) quantified the radiative errors at the SPY site using a sonic anemometer as reference temperature, and tested four correction methods. The conclusions of the T_s analysis did not change when three of the four correction methods were applied, while the fourth correction method introduced a cold bias in the data. As a result, we elected not to correct the temperature data from the naturally ventilated temperature sensors. Furthermore, by not correcting for radiative errors, the study remains relevant to sites that lack the radiation data required to correct radiative errors. In the western US, this amounts to over 75% of snow-measuring stations [*Raleigh*, 2013].

[12] Sensors at each site measured T_s (i.e., radiant snow surface temperature) either directly with an infrared sensor or indirectly through measurement of upwelling longwave radiation with a pyrgeometer. Upwelling longwave radiation was converted to T_s using the Stefan-Boltzmann equation with snow thermal emissivity (ε) equal to 1, for consistency with the published data set at CDP [*Morin et al*., 2012]. However, we note that ε may be as low as 0.97 [*Kondo and Yamazawa*, 1986], in which case reflected longwave radiation must be considered when calculating T_s from upwelling longwave data. We checked the impact of ε selection at four sites with pyrgeometers, and found that the mean difference between $T_s(\varepsilon = 1)$ and $T_s(\varepsilon = 0.97)$ was 0.2°C, and therefore, our selection of $\varepsilon = 1$ did not significantly alter the results of the study. At CDP, T_s was measured directly with an infrared thermometer and indirectly with a downward-pointing pyrgeometer; only the colder T_s measurement was reported each hour in the data set published by *Morin et al*. [2012]. A separate analysis (see supporting information 2) assessed how sensor type might impact the analysis using infrared T_s and pyrgeometer T_s measurements at the BOG site. This auxiliary analysis suggested that the type of sensor did not significantly bias the results of the study. However, due to site-to-site differences in sensor field-of-view, we qualitatively considered the impact of sensor type when interpreting the results of the study. A full assessment of the relative uncertainties of these different sensors was outside the scope of the study. Based on manufacturer's specifications, both types of sensors had temperature-dependent uncertainties in measured T_s (Table 1).

[13] Only T_s measurements in the operating ranges of the T_s sensors (i.e., −40 to 0°C for pyrgeometers, −30 to 0°C for IR sensors) were used in the analysis. T_s observations exceeding 0°C with snow cover present were manually set to the physical limit of 0°C. Averaged across the sites, these cases represented 4.6% of observations, but 19% of observations at CDP exceeded 0°C (but all were less than 2°C). These erroneous values may occur due to calibration errors, radiative heating errors, or when nonsnow surfaces (e.g., vegetation, bare ground) are located in the field-of-view of the infrared thermometer or pyrgeometer. We further constrained the analysis to periods when measured snow depth exceeded 10 cm to minimize impacts from herbaceous vegetation protruding out of the snow. Debris on the snow surface may also alter the radiometric properties of the snow, and thus presents additional uncertainty in the T_s measurements. This was relevant at CDP where tree litter and atmospheric dust have been documented [*Etchevers et al*., 2004], and at SASP and SBSP where dust deposition on the snow surface is common [*Painter et al*., 2007].

3. Calculation of Meteorological Variables and Conditions

3.1. Wet-Bulb Temperature (T_w)

[14] The wet-bulb temperature (T_w) is the temperature that an air parcel would reach if cooled to saturation at

Table 1. Site Information[a]

Site Name	Col de Porte	South Royalton	Spy Hill	Swamp Angel	Senator Beck	Opabin	Scotty Bog
Characteristics							
Acronym	CDP	SRV	SPY	SASP	SBSP	OPB	BOG
Site climate	Subalpine maritime	Continental moist	Continental prairie	Subalpine continental	Alpine continental	Moist subalpine	Permafrost wetland
Mean DJF T_a (°C)	−0.90	−5.5	−6.7	−8.5	−10	−10	−22
Elevation (m)	1325	150	1268	3371	3719	2230	283
Latitude (°N)	45.3	43.8	51.2	37.9	37.9	51.3	61.3
Country	France	USA	Canada	USA	USA	Canada	Canada
Study period	1993–2011	1991–1993	2006–2011	2003–2012	2005–2012	2006–2009	2008–2009
Data resolution	1 h	30 min	30 min	1 h	1 h	30 min	30 min
Sensors							
T_a	PT 100/3, PT 100/4 Wires	Unknown[b]	Vaisala HMP45	Campbell CS500-U	Campbell CS500-U	Vaisala HMP45	Vaisala HMP45
T_a *aspiration*	Mechanical	Natural	Natural	Natural	Natural	Natural	Natural
Humidity	Vaisala HMP35 Vaisala HMP45	Unknown[b]	Vaisala HMP45	Campbell CS500-U	Campbell CS500-U	Vaisala HMP45	Vaisala HMP45
U	Chauvin Arnoux Tavid 87	Unknown[b]	RM Young 05103	Campbell Scientific RM Young	Campbell Scientific RM Young	RM Young 05103	Met-One 014A
T_s or LW_{out} (*accuracy*[c])	Testo term Pyroterm (unknown), Heitronics KT15 (±1°C)	Net radiometer, unknown model[b] (±3°C)	Kipp and Zonen CNR1 net radiometer (±7°C at 0°C, ±6°C at −35°C)	AlpuG SnowSurf infrared thermometer (±0.5°C at 0°C, ±4°C at −35°C)	AlpuG SnowSurf infrared thermometer (±0.5°C at 0°C, ±4°C at −35°C)	Kipp and Zonen CNR1 net radiometer (±7°C at 0°C, ±6°C at −35°C)	Kipp and Zonen CNR1 net radiometer (±7°C at 0°C, ±6°C at −35°C)
Measurement Heights (m) Above Ground							
T_a and RH	1.5[d]	2.0	1.6	3.4	3.8	3.2	1.9
U	10	2.0	1.9	3.8	4.0	4.4	2.0
T_s or LW_{out}	1.2[d]	2.0	1.7	3.2	3.5	2.5	1.5

[a]Sites are sorted from warmest to coldest mean winter temperatures.

[b]Site was discontinued in 2005 and sensor records were unavailable (L. Peck, personal communication, 2013). Accuracy was taken from *Peck* [1994]. Natural ventilation was assumed for air temperature measurements at SRV.

[c]Based on manufacturer's specifications. CNR1 T_s accuracy may be better than the specification [*Van den Broeke et al*., 2004], possibly as low as ±2°C.

[d]Sensor heights were adjusted weekly to maintain consistent height above snow surface.

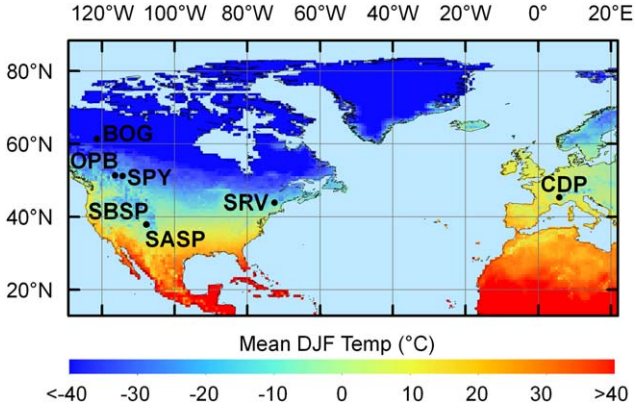

Figure 1. Sites used to evaluate snow surface temperature approximations. Acronyms are defined in Table 1. Background colors represent DJF air temperature at standard height averaged over 1900–2006 [*Legates and Willmott*, 1990].

constant pressure through evaporation of water into the parcel, where the parcel provides the latent heat for evaporation. When temperature is below the freezing point, the wet bulb is sometimes referred to as the ice-bulb temperature. T_w can be measured in the field with a sling psychrometer (which ensures convective heat transfer overwhelms radiative heat), but such measurements were not made at the sites. In the absence of measurements, T_w can be estimated with psychrometric charts or an iterative numerical approach based on temperature, humidity, and atmospheric pressure (P_{atm}). To estimate T_w, we used the iterative solution described by *Iribarne and Godson* [1981], a common tool that is used both operationally (e.g., in the Advanced Weather Interactive Processing System of the US National Weather Service) and in research models (e.g., the Distributed Hydrology Soil Vegetation Model) [*Wigmosta et al.*, 1994]. P_{atm} was estimated at a constant value using an empirical relationship between elevation and pressure at each site, except at CDP and SASP, where hourly P_{atm} measurements were available. Using observations at CDP and SASP, we tested the assumption of temporally constant P_{atm} versus hourly P_{atm} for estimating T_w, and found a maximum difference of 0.3°C between the two approaches. Thus, assuming temporally constant P_{atm} introduced little error into T_w estimation.

3.2. Dew Point Temperature (T_d)

[15] T_d is defined as the temperature that an air parcel would reach if cooled to saturation with respect to water at constant pressure without changes in moisture content. The frost point temperature is analogous to T_d, except saturation is considered with respect to an ice surface instead of water. For simplicity, we refer to both as T_d, but note that we are actually calculating frost point when $T_a \leq 0$°C and the dew point when $T_a > 0$°C. Here we assume that there is no freezing-point depression for liquid water, and that the water vapor and snow have no impurities. For an unsaturated air parcel, T_d is lower than the other standard temperatures, where $T_d < T_w < T_a$. For a saturated air parcel (i.e., $e = e_{sat}$), $T_d = T_w = T_a$.

[16] T_d can be measured with a variety of hygrometers (e.g., capacitive, resistive, chilled mirror), but often saturation state or moisture content is instead reported as relative humidity (RH) or specific humidity in published data sets. We, therefore, used a Magnus-Tetens approach [*Murray*, 1967] to convert measured T_a (°C) and fractional RH to T_d (°C) at each time step:

$$T_d = \frac{c\left[\ln(RH) + \frac{bT_a}{c+T_a}\right]}{b - \ln(RH) - \frac{bT_a}{c+T_a}} \quad (1)$$

[17] *Alduchov and Eskridge* [1996] provide different empirical coefficients for equation (1) depending on whether saturation is taken with respect to water ($e_{sat,w}$) or with respect to ice ($e_{sat,i}$). When $T_a > 0$°C, we use the $e_{sat,w}$ coefficients $b = 17.625$ and $c = 243.04$°C, and when $T_a \leq 0$°C, we use the $e_{sat,i}$ coefficients $b = 22.587$ and $c = 273.86$°C. Relative to other common approximations, maximum relative error with this approach is 0.384% for calculating vapor pressure [*Alduchov and Eskridge*, 1996]. This maximum error in e_{sat} translates to a maximum error of 0.1°C in T_d. Because of the high precision of this empirical equation, uncertainty in T_d arises almost exclusively from uncertainties in measured T_a and RH.

3.3. Boundary Layer Stability

[18] We hypothesize that atmospheric stability plays a complex role in the representation of T_s with standard height temperatures. *Andreas* [1986] hinted at this by showing that near-surface T_d theoretically approached T_s as latent heat flux decreased to 0 W m^{-2}, and the absolute different between T_d and T_s decreased with increasing wind speed. This implies that T_d approximates T_s best under periods with (1) high wind shear (i.e., by proxy, unstable boundary conditions) or (2) when there is no vapor pressure gradient between the near-surface atmosphere and the snow surface (i.e., no sublimation or condensation). He also showed that when T_d was less (greater) than T_s, sublimation (condensation) was occurring at the snow surface. However, he did not explicitly consider the role of atmospheric stability. We expect that T_d at standard height best represents T_s during unstable conditions when turbulent mixing reduces stratification of moisture and temperature. During stable conditions, standard height temperatures can become decoupled from T_s.

[19] To characterize boundary layer stability, we calculated the bulk Richardson number (Ri_b) [*Singh and Frevert*, 2002] at each time step:

$$Ri_b = \frac{gz(T_a - T_s)}{0.5(T_a + T_s)U(z)^2} \quad (2)$$

where g is the acceleration of gravity (m s^{-2}), z is the height of the temperature sensor above the snow surface (m), temperature values are in Kelvin, and $U(z)$ is wind speed (m s^{-1}) at height z. Because wind speed was not measured at the same height as temperature at every study site (Table 1), we rescaled the measured wind speed (U_{obs}) to the temperature sensor's height z at each time step assuming a power law wind profile:

$$U(z) = U_{obs}\left(\frac{z}{z_u}\right)^{\alpha} \quad (3)$$

where z_u is the height of the wind speed measurement (m) and α is 1/7, an average value assumed when the wind profile is unknown [*Peterson and Hennessey*, 1978]. A potential source of error in this rescaling approach arises when the near-surface wind profile deviates from the power law profile, such as during periods of shallow katabatic flow [*Whiteman*, 2000]. The sites did not collect wind profile data that would permit better understanding of these errors.

[20] The Richardson number compares buoyancy suppression of turbulence against turbulence generation to characterize stability conditions. Based on the literature, a critical Richardson number in the 0.15–0.25 range separates unstable and stable conditions, with unstable (stable) conditions prevailing below (above) the critical value. We assume that the critical number is 0.20 at the study sites, but note that there is disagreement about the critical number over snow [for a discussion, see *Andreas*, 2002]. We note that many physically based snow models [e.g., *Jordan*, 1991] implement a correction based on Ri_b when computing turbulent fluxes.

3.4. Radiative Heating and Clearness Index

[21] Because incoming radiation is the primary energy source for heating and melting a snowpack in many climates, it is important to consider how radiative heating impacts T_s and approximations thereof. Solar heating of instruments may also bias measurements of T_s [*Andreas*, 1986] and standard height temperature [*Huwald et al*., 2009]. Incoming shortwave and longwave radiation vary with latitude, slope, elevation, time of day, time of year, forest cover, and cloud cover. For simplicity, we only consider how radiation changes in time and with sky conditions (i.e., clearness versus cloudiness). To approximate sky conditions, we calculated a dimensionless clearness index (*CI*) at each time step:

$$CI = \frac{Q_{si,obs}}{Q_{si,toa}} \quad (4)$$

where $0 \leq \mathrm{CI} \leq 1$, $Q_{si,obs}$ is measured incoming shortwave radiation (W m^{-2}) and $Q_{si,toa}$ is extraterrestrial incoming shortwave radiation (W m^{-2}), which varies latitudinally, diurnally, and seasonally. $Q_{si,obs}$ was observed at all sites; however, we used the SBSP observations at SASP because of the tendency for the radiometer dome to become snow covered at SASP where it is less windy than SBSP. $Q_{si,toa}$ was calculated as a function of time of day, time of year, and latitude [*Iqbal*, 1983]. High values of *CI* indicate sunny conditions during the day, and surface cooling at night. We classified cloudy conditions when $CI < 0.35$ and sunny conditions when $CI > 0.35$ based on *Musselman et al*. [2012]. Because *CI* was only used to classify cloudy versus clear sky conditions, we expected minimal impact in the *CI* analysis from topographic shading. At sites and times of the year where topographic shading was important, this effect was similar to cloudy conditions near sunrise or sunset. Note that *CI* (equation (4)) and the Richardson number (equation (2)) are calculated independently of each other.

[22] Equation (4) does not yield valid *CI* values during the night. Following the recommendations of *Flerchinger et al*. [2009], we applied a 24 h averaging window to $Q_{si,obs}$ and $Q_{si,toa}$ before calculating *CI*. This yielded values at night based on clearness conditions from the previous and following days, making it less sensitive to Q_{si} errors at sunrise and sunset. Manual observations of sky conditions were not available, so it was not possible to provide uncertainty estimates of this interpolation. However, qualitative comparison with *CI* back-calculated from local Q_{li} measurements showed that the Q_{si}-based *CI* calculations reasonably represented temporal variations in clearness conditions (no figures shown). More research is needed to better understand the uncertainty in the nighttime CI.

3.5. Evaluation Metrics

[23] We quantified how well T_a, T_w, and T_d each approximated T_s according to three metrics. These metrics included the coefficient of determination (R^2), mean bias, and root-mean-squared error (RMSE). The R^2 statistic measures the variance explained in the T_s time series by each temperature time series, providing a measure of the temporal correlation between data sets.

[24] Mean bias reflects the systemic difference between two data sets and how accurately one represents the other. Mean bias (°C) was calculated as:

$$\mathrm{bias} = \frac{1}{n}\sum_{i=1}^{n} Tx(i) - Ts(i) \quad (5)$$

where n is the number of hourly observations at each site with snow cover (i.e., depth > 10 cm), and T_x is the temperature approximation (i.e., T_a, T_w, or T_d).

[25] RMSE measures the random differences between two data sets and the level of precision when approximating one data set with another. RMSE (°C) was calculated as:

$$\mathrm{RMSE} = \sqrt{\frac{1}{n}\sum_{i=1}^{n} (Tx(i) - Ts(i))^2}. \quad (6)$$

[26] Statistics are reported for each site separately. When considering the aggregate statistics across all sites, we first calculated the statistics for each site and then averaged them because the sites had varying periods of record and different sampling frequencies (Table 1).

4. Physically Based Snow Modeling Experiment

[27] To illustrate how a simple, independent approximation of T_s might benefit snow modeling studies, we considered how biases in the energy balance of a physically based snow model become manifested in T_s and whether T_d can be used to detect bias. This was a relevant application, as data are rarely available to validate the energy balance or T_s in snowmelt modeling studies. We selected the one-dimensional, multilayer snow thermal model (SNTHERM) [*Jordan*, 1991] for the physically based simulation of T_s at the CDP site during water year 2006. SNTHERM was developed specifically for the prediction of T_s (i.e., the thermodynamic temperature of the top layer) based on energy

exchanges at the snow-atmosphere interface and is regarded as one of the more sophisticated and reliable snow models available [*Etchevers et al*., 2004]. SNTHERM simulates various snowpack processes, including snow accumulation, frost development, compaction, metamorphosis, grain growth, sublimation, and snowmelt. *Watson et al*. [2006] argued that SNTHERM is the "benchmark model" for physically based simulation of snowmelt processes, though the model's complexity has limited its application in distributed modeling.

[28] SNTHERM simulates snowpack development by dividing new snowfall into horizontally infinite layers. The governing equations for energy and mass balance are applied between these layers, with the meteorological conditions applied at the upper (i.e., snow-atmosphere) boundary, and steady state conditions assumed at the lower (i.e., snow soil) boundary. An iterative numerical solution yields estimates of T_s, and layer specific states for thickness, density, temperature, and phase. Iterative solution of T_s from the energy balance is possible because multiple processes are functions of T_s, including outgoing longwave radiation, sensible heat, latent heat, and heat conduction into the snowpack [*Outcalt*, 1972; *Outcalt et al*., 1975; *Jordan*, 1991; *Tarboton and Luce*, 1996; *Liston and Elder*, 2006]. Physically based, iterative approaches for estimating T_s have disadvantages in that they require accurate forcing data for the other components of the energy balance [*Pomeroy et al*., 1998], and they can be computationally expensive to reach convergence [*Wigmosta et al*., 1994]. Despite being physically based, some parameters in these models require calibration (e.g., thermal conductivity) [*Tarboton and Luce*, 1996; *Essery and Etchevers*, 2004], which yields additional uncertainties in modeled T_s and the surface energy balance.

[29] To demonstrate the relationship between energy balance bias and T_s bias, we simulated snowpack at CDP during one water year with SNTHERM, with a control simulation and with biased forcing data scenarios. For the control simulation, we used local hourly observations (i.e., T_a, RH, wind speed, incoming shortwave radiation, outgoing shortwave radiation, and incoming longwave radiation) to force the model and compared modeled and observed values of T_s. This provided a benchmark for understanding the accuracy of modeled T_s under an ideal forcing data scenario. We also compared T_d and T_s as a reference. We then introduced artificial biases (−15%, −10%, −5%, +5%, +10%, +15%) in the incoming radiation data and then modeled T_s with SNTHERM with each of these six biased data sets. Biases were applied to daytime hours only for shortwave radiation and at all hours for incoming longwave radiation. These scenarios with biased radiation resembled the reality of snowmelt modeling in a data sparse environment, as biases in model data and/or parameters can propagate to model outputs (e.g., T_s, SWE) in ways that are not easily detected. We then compared the T_s simulations generated with biased model data against both measured T_s and T_d to determine whether these yielded similar relationships. To determine whether T_d could be used to detect bias in a snowmelt model, we examined the relationship between the energy balance biases and the mean difference between modeled T_s and T_d. All temperature values were aggregated from hourly to daily mean values in this experiment for simplicity. Finally, we conducted an auxiliary analysis to determine how the thickness of the top snow layer impacts T_s approximation (see supporting information 3), so as to make the results relevant to other snow models (e.g., SNOBAL [*Marks et al*., 1998]) that make the top layer thickness constant in time. This separate analysis indicated that the approach may be generally applicable to other models as long as the top layer is thin ($\leq$5 cm).

5. Results and Discussion

5.1. Comparing Radiant T_s With Standard Height Temperatures

[30] Comparisons of the standard height hourly temperatures (T_a, T_w, and T_d) and observed radiant T_s are presented in Figure 2. For all temperature comparisons, much of the scatter in Figure 2 is due to subdaily variations. For each site, summary statistics are shown for hourly values in Figure 3 and daily maxima/minima in Figure 4. Diurnal statistics for all sites are shown in Figure 5. We now address each temperature data set sequentially through these figures.

[31] Despite reasonable correlation between T_a and T_s, T_a was consistently higher than T_s, and the magnitude of this bias was inconsistent between sites (Figures 2a–2g, and 3b). Averaged across the sites, $T_a > T_s$ in 95% of measurements; convective instability is rare in snow-covered environments, which helps explain why T_a is generally biased high for T_s estimation. For T_a, we also considered lagged correlations with T_s, but found that the greatest correlation was with no lag at four of the seven sites. T_a approximated T_s better during daytime than during night, as indicated by the three summary statistics (Figure 5).

[32] Like T_a, T_w also exhibited a consistent warm bias (Figure 3b), although this bias decreased with increasing T_s (Figures 2h–2n). Despite this warm bias, T_w had the strongest correlation with T_s at all sites (Figure 3a) and at all hours of the day (Figure 5a). The correlation improved slightly at only two of the seven sites when a lag correlation was attempted (no figure shown). The strength of the correlation between T_w and T_s appeared related to the diurnal cycle, as the correlation was comparable to the T_d correlation at night but increased slightly during the daytime hours, while the strength of the T_d correlation diminished during the day (Figure 5a). However, it was not clear why this occurred. One possible explanation is that sublimation from the snowpack during the day released vapor into the air above, such that T_w tracked these variations. The vapor pressure of the air tended to increase during daytime, which supports this hypothesis (no figures shown).

[33] Of the three standard height temperatures, T_d had the lowest absolute bias and RMSE when approximating T_s (Figures 3b and 3c), but underestimated T_s more often than T_a and T_w at warmer T_s (Figures 2o–2u). The correlation between T_d and T_s was never stronger than the correlation between T_w and T_s at any one site (Figure 3a) or during daytime hours (Figure 5a). Mean $T_d - T_s$ ranged from −2.3 to +2.6°C across the sites and from −2.8 to 1.5°C across the diurnal cycle (when averaged across all sites). These ranges exceed the ±1°C accuracy reported by *Andreas* [1986] when using 10 cm height T_d. However, at four sites (SPY, SASP, OPB, BOG), the bias ranged from −1.0 to

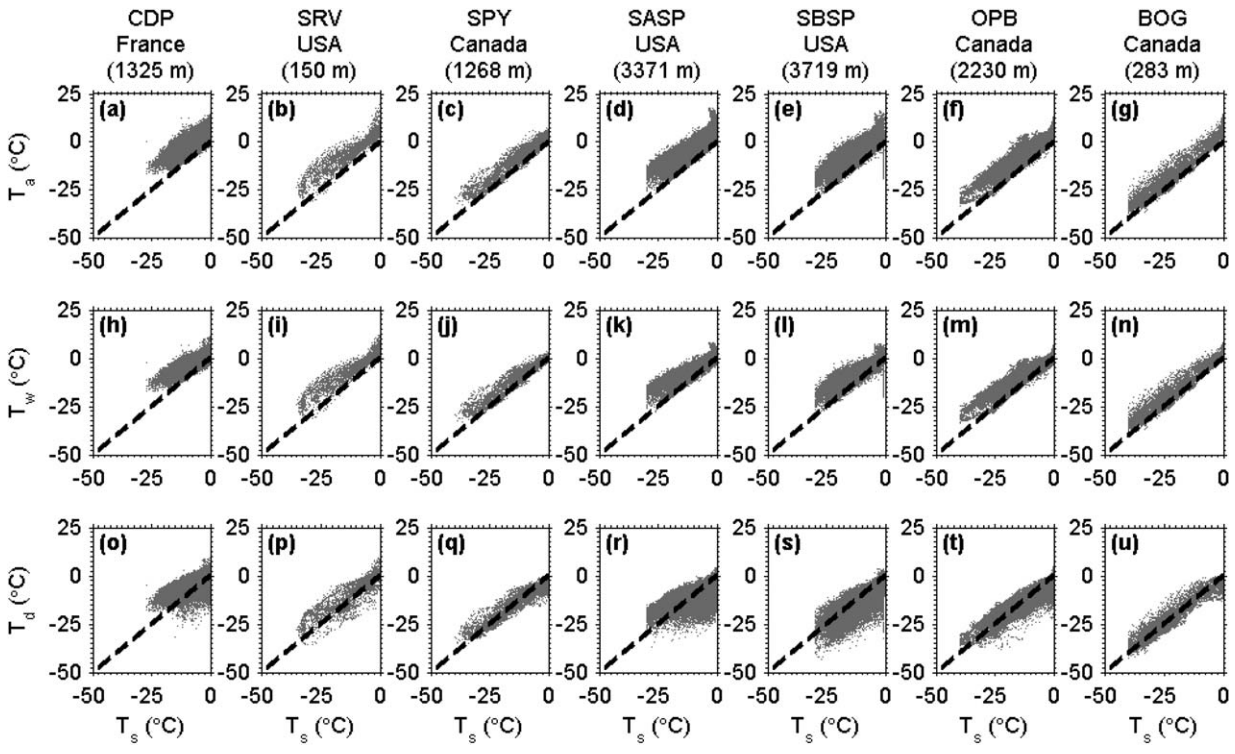

Figure 2. Comparisons between observed subdaily (i.e., 30 min or hourly) snow surface temperature (T_s) and standard height (a–g) air temperature, (h–n) wet-bulb temperature, and (o–u) dew point temperature at the seven study sites. The sites are organized from warmest (left) mean DJF temperatures to coldest (right). Comparisons are only shown during periods when snow depth exceeded 10 cm and when T_s was within the measurement range. The black dashed line is the 1:1 line.

−0.3°C, well within the range of *Andreas* [1986]. Thus, climate and environmental conditions may play as large of a role in the bias as the measurement height of T_d. It is also important to note that the absolute bias for approximating T_s with T_d is comparable to the statistics reported for more sophisticated snow models [*Brun et al*., 1989; *Boone and Etchevers*, 2001] that solve T_s but require far more data (e.g., incoming shortwave and longwave radiation, wind speed). However, the RMSE of the T_d approximation (3.3–5.8°C) was higher than the RMSE of these sophisticated models (typically $\leq$3°C).

[34] In approximating daily maxima and minima of T_s, the saturation temperatures (i.e., T_w and T_d) provided improved representation over T_a (Figure 4). At all sites, T_a overestimated daily maxima and minima of T_s. At five of the seven sites, maximum daily T_s values were typically between T_w and T_d (Figure 4a). Both T_w and T_d overestimated minimum daily T_s at all sites, except at SBSP, where T_d underestimated minimum daily T_s (Figure 4b). Daily minimum T_s was typically colder than daily minimum T_d, suggesting that stable conditions at night decoupled standard height T_d and T_s (see section 5.2). This relationship was not captured in the composite analysis of diurnal temperature (Figure 5) because the timing of minimum T_d and T_s did not always coincide and because the minimum values varied both temporally and from site-to-site.

[35] The results indicate that to first order, T_d represents daily average T_s (Figure 3), minimum daily T_s (Figure 4b), and nighttime T_s (Figure 5b) with the least bias, and that

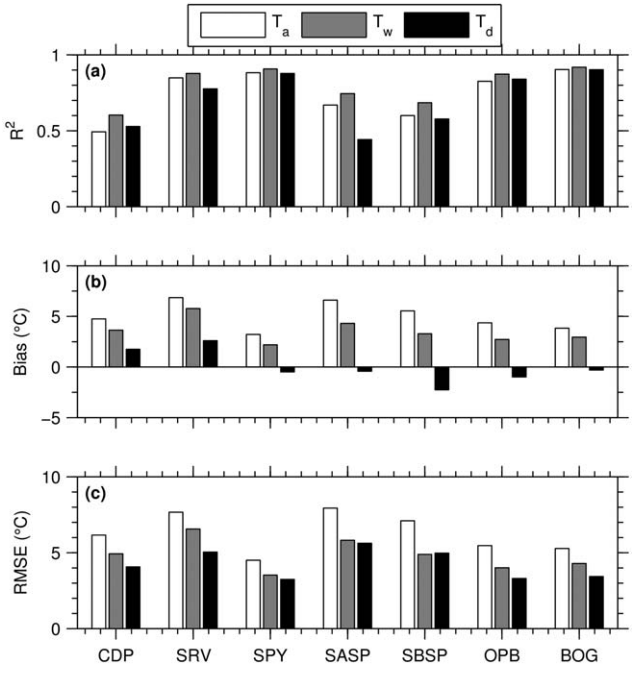

Figure 3. Summary statistics, (a) R^2, (b) Bias, and (c) RMSE, for approximating hourly snow surface temperature with air temperature, wet-bulb temperature, and dew point temperature at the seven study sites.

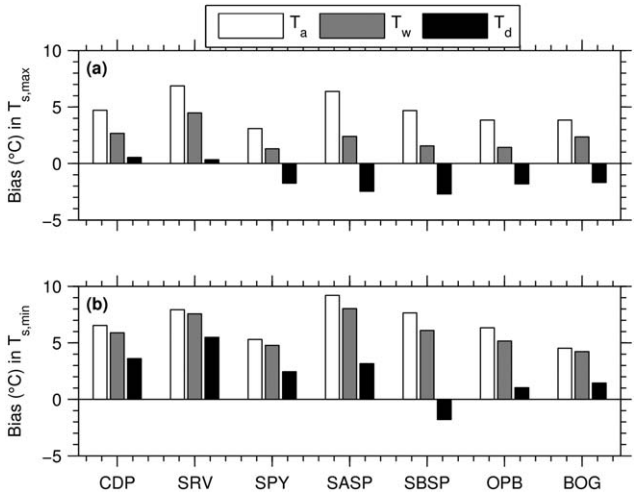

Figure 4. Bias in estimating (a) maximum daily surface temperature ($T_{s,max}$) and (b) minimum daily surface temperature ($T_{s,min}$) using air temperature (T_a), wet-bulb temperature (T_w), and dew point temperature (T_d) at the seven study sites. A positive bias indicates overprediction of T_s.

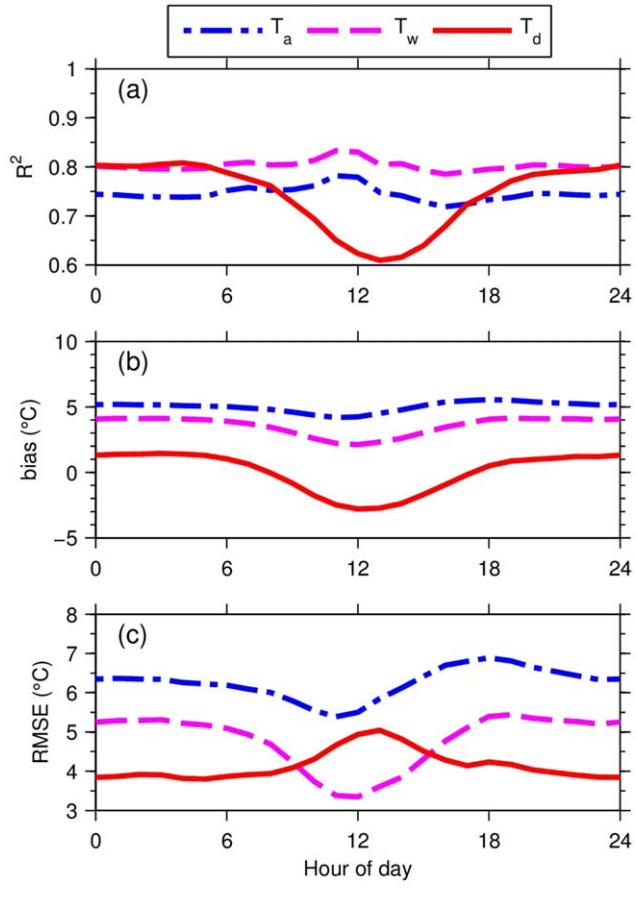

Figure 5. Summary statistics for approximating hourly snow surface temperature with air temperature, wet-bulb temperature, and dew point temperature at all study sites as a function of time of day. Statistics were first computed for each hour at each site, and then the diurnal statistics were averaged across sites.

Table 2. Mean Daily Temperature Ranges[a] (°C) at the Study Sites During Periods with Snow Depth Exceeding 10 cm

	CDP	SRV	SPY	SASP	SBSP	OPB	BOG
T_s	**8.4**	**15**	**12**	**15**	**11**	**9.1**	**15**
T_a	6.2	14	9.2	12	7.8	6.4	14
T_w	4.6	11	7.8	8.8	6.2	5.1	12
T_d	4.9	9.9	7.5	9.1	10	6.3	11

[a]At each site, the largest temperature range is in bold.

the saturation temperatures (T_w and T_d) characterize maximum daily T_s more accurately than T_a. None of the standard height temperatures captured both the daily maxima and minima of T_s because their diurnal ranges tended to be much lower than the T_s diurnal range (Table 2). Approximation of hourly T_s might thus be improved using T_w during the day and T_d during the night as predictors (Figure 5), but development of such a method was outside the scope of this study.

[36] These comparisons demonstrate the inherent difficulty in estimating T_s based on T_a across different climates. While $T_a = T_s$ (top layer) may be true under certain meteorological conditions at night [see *Helgason and Pomeroy*, 2012, Figure 9], the results of this study (which span a wider range of seasonality and climate) indicate that these conditions are not frequent and that generally $T_a > T_s$. Empirical methods of estimating T_s based on a static offset from T_a [e.g., *Brubaker et al.*, 1996] attempt to correct the estimation bias, which ranged from +3.2 to +6.8°C at the seven study sites and from +4.4 to +5.5°C across the diurnal cycle. However, the bias cannot be known a priori, and can vary from published values even within a single climatic zone. For example, *Brubaker et al.* [1996] found that T_a was typically +2.5°C higher than T_s at a site in Vermont, USA, but our data in Vermont (SRV) suggests the difference is +6.8°C. Using the 2.5°C offset, a bias of 4.3°C would remain, exceeding the 2.6°C bias found from assuming that T_d approximated T_s. We, therefore, expect methods that estimate T_s based on an offset from T_a have limited usefulness due to a lack of transferability.

5.2. Impacts of Stability and Radiation on Radiant T_s Approximation

[37] Because radiation interacts with boundary layer stability through surface heating, it is difficult to distinguish their independent effects. We used a compositing approach to examine how each of these factors contributed to bias when approximating radiant T_s with standard height T_d. We only consider T_d for the rest of the study because it approximated T_s with the lowest bias at all sites and the lowest RMSE at most sites (section 5.1). To assess the role of stability, we first calculated the difference between T_s and T_d and binned the results using the critical Ri_b as a classifier (Figure 6). Relative to unstable conditions, the difference between T_d and T_s tended to increase during stable conditions, such that T_s was generally colder than T_d. Such a cooling effect may arise at night due to surface cooling or during the day due to shallow stable layer formation over melting snow cover [*Halberstam and Schieldge*, 1981; *Mahrt and Vickers*, 2005]. Median $T_d - T_s$ was closest to 0°C during unstable conditions at five of the sites with statistical significance (95% level, rank sum test).

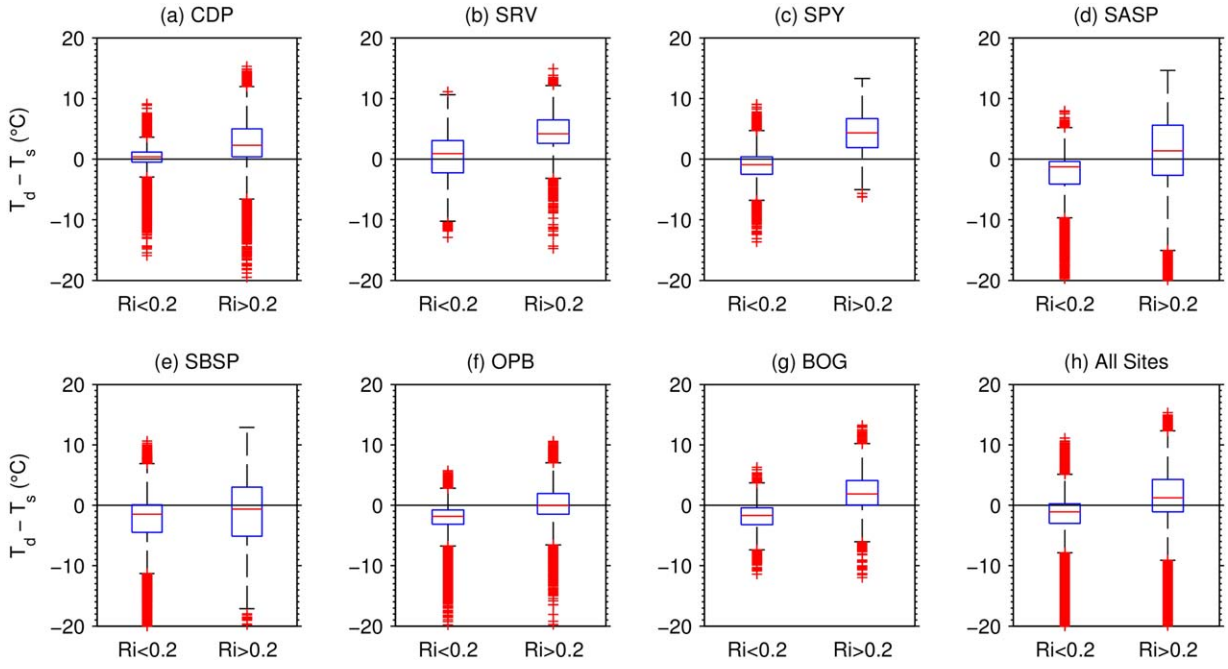

Figure 6. Box plots showing the difference between dew point temperature (T_d) and measured snow surface temperature (T_s) as a function of the bulk Richardson (Ri_b) number at the seven study sites. Hours are binned based on unstable ($Ri_b < 0.2$) and stable ($Ri_b > 0.2$) conditions. T_d data are constrained to an upper limit of 0°C for prediction of T_s.

[38] Averaging the hourly bias across the sites provided further clarification on how radiation and stability each affected approximations of T_s with T_d (Figure 7). Clear sky periods generally had $T_d > T_s$ at night and $T_d < T_s$ during the day (Figure 7a). Cloudy periods had similar differences between T_s and T_d at night, but smaller differences between T_s and T_d during the day. The midday underestimation bias was a persistent feature at most of the sites when approximating T_s with T_d. Stable periods decoupled T_s and T_d at night, such that T_s was 3.0°C colder than T_d when averaged across nighttime hours and across all sites (Figure 7b). In contrast, T_s measurements were typically within 0.5°C of T_d during unstable periods at night. Regardless of stability conditions, the effect of radiative heating caused $T_s > T_d$ during the daytime hours. When considering stability and radiation conditions together (Figure 7c), cloudy and unstable periods had the lowest bias through the day. The midday (i.e., noon) bias was most reduced during cloudy and stable periods, but this was likely the result of offsetting effects from surface cooling (due to stable conditions) and surface heating (due to radiation).

[39] The frequency of stable conditions and clear skies helped explain why approximating T_s with standard height T_d was more reliable at some sites and less reliable at others (Figure 8). Bias in approximating T_s with T_d at midday was significantly ($p < 0.01$) related to the frequency of clear sky conditions (Figure 8a); the sunniest sites (e.g., SASP and SBSP) had the largest noon bias when approximating T_s with T_d. At midnight, bias in the approximation was significantly related to stability frequency (Figure 8b, $p = 0.05$). The midnight bias was closer to 0°C at windy sites where stable conditions were less frequent (e.g., SBSP, SPY, and OPB). The type of T_s instrument did not seem to impact the results (Figure 8 and see supporting information 2).

[40] Because T_d approximates T_s less reliably under stable atmospheric conditions (Figures 6–8), it would be difficult to calculate the bulk Richardson number (Ri_b) accurately at locations where only temperature and humidity observations were available. In the above analysis, we computed Ri_b using measured T_s in equation (2). In practice, Ri_b would need to be computed with an assumed value of T_s and an estimate of wind speed. The assumption of $T_s = T_d$ results in increased uncertainty in Ri_b, as T_d tends to overestimate T_s during the night and underestimate T_s during the day for stable conditions. This propagates error into the calculated Ri_b, thereby obscuring understanding of the stability and turbulence conditions and the reliability of the $T_s = T_d$ approximation at a given time. To quantify this issue, we compared categorical estimates of stability (i.e., stable versus unstable) in time using Ri_b values calculated from T_s and Ri_b values calculated from T_d, assuming wind speed was known. Averaged across the sites, $Ri_b(T_d)$ correctly identified stable conditions 30% of the time (min = 5%, max = 56%) and correctly identified unstable conditions 55% of the time (min = 27%, max = 88%). When identifying unstable conditions, $Ri_b(T_d)$ matched $Ri_b(T_s)$ reasonably at the prairie SPY site (88% correct) and at the alpine SBSP site (83% correct), but $Ri_b(T_d)$ did not often match $Ri_b(T_s)$ at the wind-sheltered SASP site (27% correct). While we are unable to resolve this issue with uncertainty in Ri_b, this analysis shows the identification of unstable periods (when $T_d = T_s$ is more reliable) is least impacted at windy, exposed sites.

[41] *Andreas* [1986] originally found that daytime T_d was lower than T_s on sunny days, but assumed that solar heating biased the infrared sensor that he used to measure T_s.

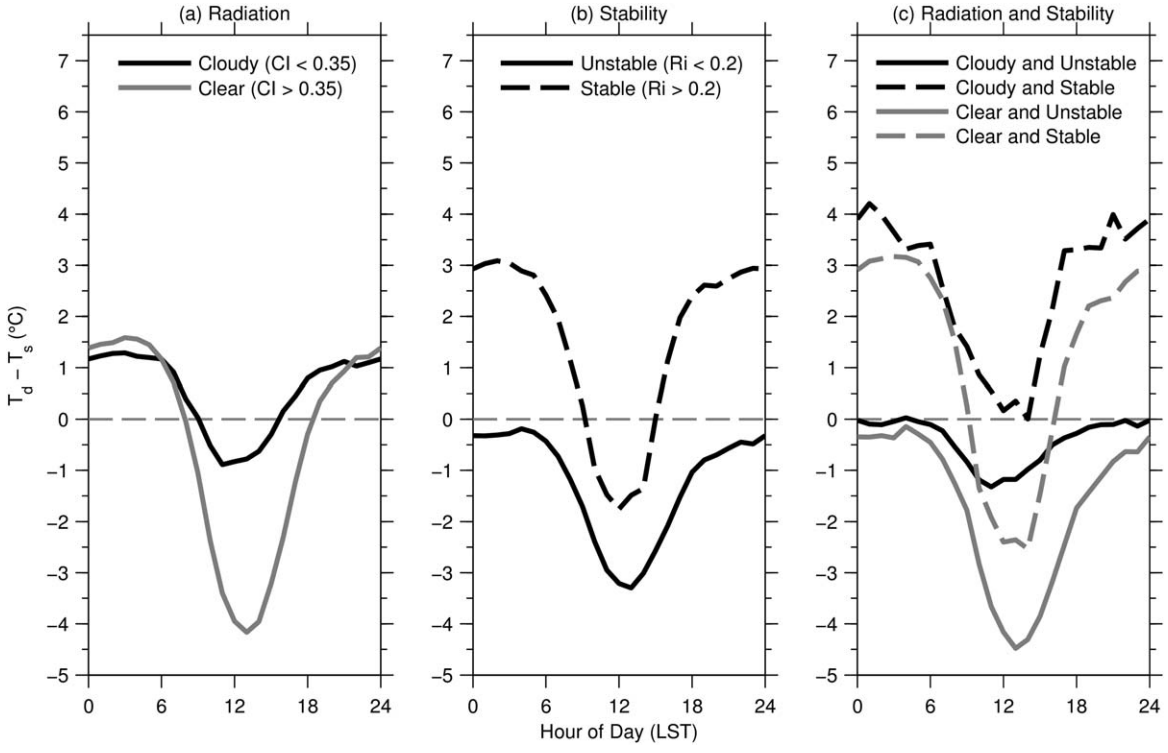

Figure 7. Difference between dew point temperature and measured snow surface temperature averaged across all seven sites during each hour of the day. Results are classified based on (a) radiation conditions (as defined by the clearness index, *CI*), (b) stability conditions (based on critical bulk Richardson number, Ri_b), and (c) both radiation and stability conditions. T_d data are constrained to an upper limit of 0°C for prediction of T_s.

Radiative heating presents a source of uncertainty in the T_s measurements of our study and may explain some of the midday bias in approximating T_s with T_d. However, we also note that snow has been shown to exhibit remarkable fluctuations in temperature over subdaily time scales in response to fluctuations in energy. In a controlled laboratory experiment, *Shea and Jamieson* [2011] documented that for a moderately dense snowpack (i.e., 270 kg m^{-3}), T_s increased 14°C in response to 3 min of 175 W of infrared heating, and cooled back to the original temperature minutes after the heat source was removed. The field observations of *Wagner and Horel* [2011] also showed that T_s can exhibit large diurnal fluctuations, with temperature increasing from −17 to −0.3°C over a 6 h period. Our temperature data (Table 2) indicate that daily ranges of T_s were within these carefully measured values, and therefore, we cannot attribute all of the daytime bias to solar heating of the T_s sensors. With the available data, we cannot distinguish T_s measurement errors from actual increases in T_s. However, simulations with the physically based SNTHERM model indicate that the magnitude of these midday surface temperature fluctuations are plausible, supporting the hypothesis that the observed increases in T_s are not the result of sensor heating (no figures shown).

5.3. Thermodynamic T_s Case Study: Comparisons With SNTHERM

[42] The top layer thermodynamic T_s from the SNTHERM control simulation (i.e., all forcing data available) accurately represented radiant T_s at CDP in water year 2006, with $R^2 = 0.97$, bias = +0.74°C, and RMSE = 1.14°C for mean daily T_s (Figure 9a). The control simulation tended to overestimate radiant T_s mostly at colder temperatures but matched T_s better as the snow warmed to the melting point. These results demonstrate that a sophisticated snow model can produce realistic simulations of T_s under an ideal data input scenario.

[43] In comparison, the simple approximation of radiant T_s with T_d (Figure 9b) yielded a similar bias in modeled T_s (bias = +1.02°C), although this T_d approximation had higher variability ($R^2 = 0.75$ and RMSE = 2.7°C), especially at colder temperatures. While the accuracy of the T_d approximation was lower than the snow model, it was accomplished with fewer data inputs (i.e., only temperature and humidity). The biases of both approaches (Figures 9a and 9b) are comparable to the highest accuracy (±0.7°C) obtained with multiple snow models in the snow model intercomparison project [SnowMIP, *Etchevers et al.*, 2004]. The RMSE of the T_d approximation is also within the 0.7–3°C RMSE range reported for most models in SnowMIP and the 0.79–2.88°C RMSE range for three models tested by *Boone and Etchevers* [2001].

[44] Artificial biases introduced in the energy balance were directly correlated with the resulting bias in SNTHERM-modeled T_s, such that underestimation (overestimation) biases in the energy balance yielded underestimation (overestimation) biases in T_s. Examples for the cases of ±10% bias are shown in Figures 9c–9f. Interestingly, similar biases were observed when comparing modeled T_s to observed T_s and T_d in the −10% energy bias case

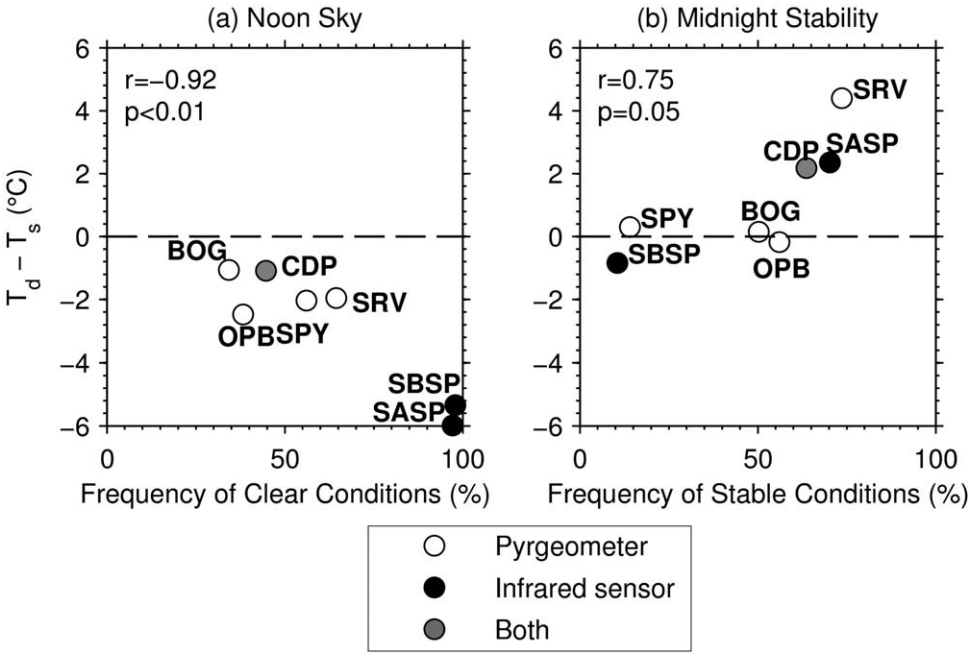

Figure 8. Frequency of (a) noon clear sky conditions and (b) midnight stability versus mean bias when approximating T_s with T_d at (a) noon and (b) midnight. T_d data are constrained to an upper limit of 0°C for prediction of T_s. Noon is taken as the average from 1100 to 1300 h, while midnight is taken as the average from 2300 to 0100 h. The markers denote the type of instrument used to measure T_s.

(Figures 9c and 9d), and when comparing modeled T_s to observed T_s and T_d in the +10% energy bias case (Figures 9e and 9f). In fact, the bias in the energy balance was strongly correlated ($p < 0.001$) with the mean difference between modeled T_s and T_d (Figure 9g). Because T_d is a reasonable surrogate for T_s for daily averages (Figure 3b), the implication is that T_d has potential use as a diagnostic tool for detecting bias when simulating snowpack with a physically based model.

[45] Our results suggest that large systematic differences (i.e., exceeding 2°C) between modeled T_s and T_d may indicate the presence of bias in the energy balance. Although this does not reveal the source of the bias (e.g., model parameters, forcing data), it provides a previously unrealized method for assessing bulk model performance. Energy balance bias is common in mountains and snow-dominated environments because most components require estimation, and it is difficult to estimate radiation accurately in complex terrain. For example, *Jepsen et al*. [2012] showed absolute biases in modeled downwelling radiation as high as 30% (for shortwave) and 15% (for longwave) over the March to August snowmelt period in the Sierra Nevada and Rocky Mountains. T_d could help detect biases of these magnitudes in the energy balance. More work is needed to develop this methodology, but the results from this example show promise for distributed model testing in data scarce regions.

6. Summary and Conclusions

[46] In this study, we assessed how standard near-surface measurements of temperature and humidity (T_a, T_w, T_d) compared to measured values of T_s. We examined how site climate, time of day, boundary layer stability, and radiation impacted T_s representation. We further compared T_s approximations based on T_d against T_s simulations from a physically based, energy balance snowmelt model (SNTHERM), and demonstrated that T_d can be used to detect bias in the modeled snowpack energy balance. The goal was to provide a practical extension of the work of *Andreas* [1986] in order to understand how well standard height dew point temperature approximates T_s (both radiant and thermodynamic) over a wider range of conditions. The results demonstrated that the standard height saturation temperatures (T_w and T_d) approximated T_s more accurately than T_a (Figures 2–5). However, T_d tended to underestimate maximum daily T_s and (at most sites) slightly overestimate minimum daily T_s (Figure 4). Biases were related to the frequency of stability and radiation conditions, and these effects varied with time of day and the frequency of those conditions (Figures 6–8). Results from a modeling case study showed that approximating T_s with T_d is a potential tool for diagnosing forcing data bias in an energy balance model (Figure 9).

[47] We, therefore, conclude that T_d at standard height is a reasonable first-order approximation of daily average T_s in many environments, and that it is preferred over approaches that track T_a, which have seen more usage in the literature. The modeling experiment results indicate that comparing mean daily T_d to model estimates of mean daily T_s across the snow season has previously unrealized value for assessing model performance in mountains and snow-dominated areas, where evaluation data are rarely found at the location of interest. It was beyond the scope of this study to test this model diagnostic tool comprehensively, and future work should develop the method further.

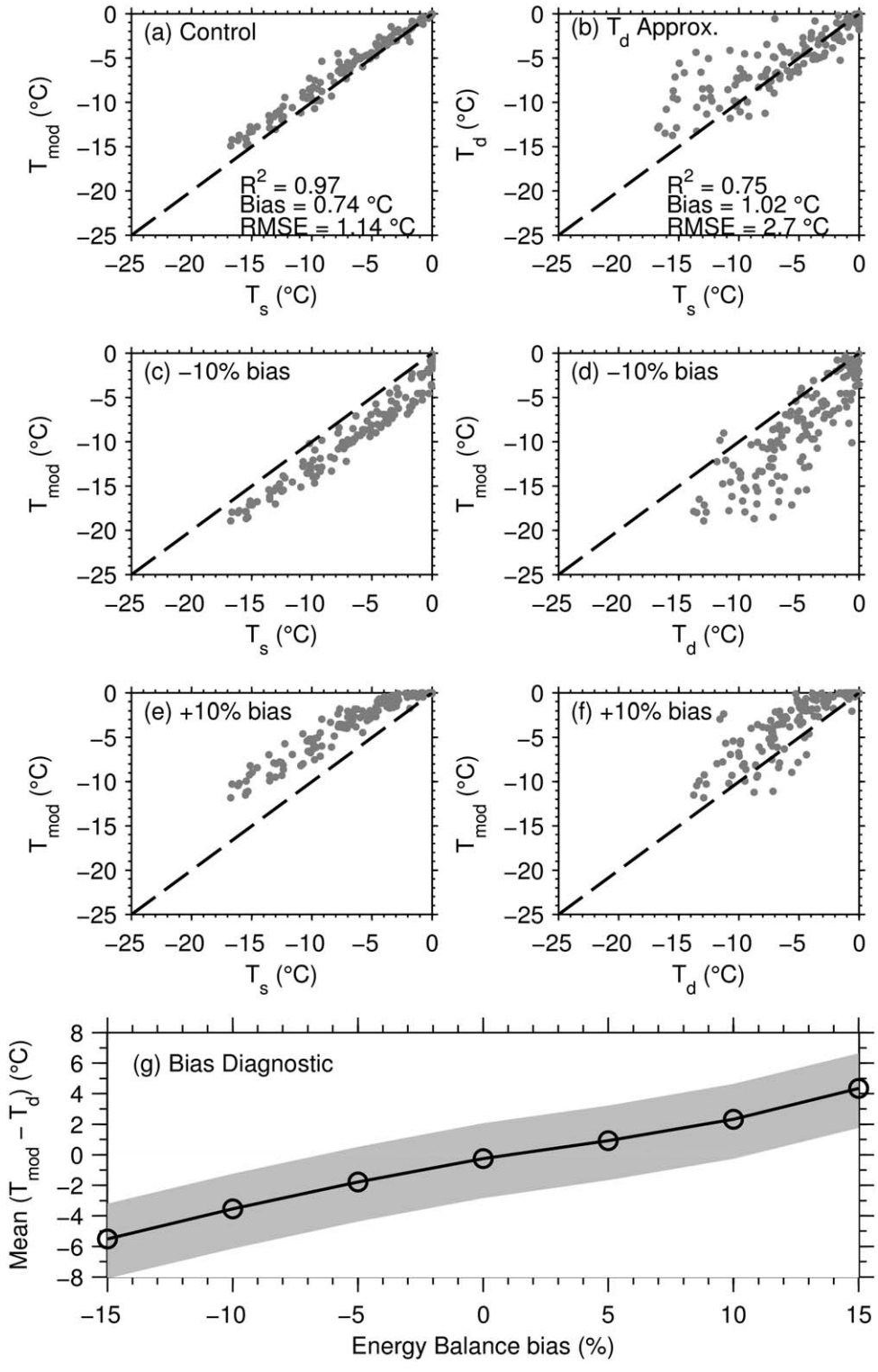

Figure 9. Modeling experiment results with SNTHERM at CDP in water year 2006. Shown are (a) the control model simulation (no bias introduced in model data) and (b) the approximation of T_s with T_d. (c–f) Examples of ±10% energy balance bias, where Figure 9c compares modeled T_s (−10% radiation bias) to observed T_s, and Figure 9d compares modeled T_s (−10% radiation bias) to T_d. Figures 9e and 9f are the same as Figures 9c and 9d except for +10% radiation bias in the model. (g) The relationship between energy balance bias (%) and the mean difference between modeled T_s with T_d . The shading in Figure 9g represents the −2.3 to +2.6°C uncertainty range when approximating observed T_s with T_d, as found in this study. Only mean daily values are shown.

Based on the results here, we expect that approximating T_s with T_d is most robust in climates and times where insolation is low and at locations where turbulent mixing occurs frequently (e.g., alpine areas, windy ridges). Windy regions in alpine, prairie, and Arctic environments areas may present the most ideal testing grounds for remotely sensed T_s with spatially distributed T_d, as remote sensing of snow properties is possible in these environments. Due to a lack of measurements in forested sites, we cannot extrapolate the results of this study to locations under forest canopies, where turbulence and radiation dynamics are altered due to wind sheltering and canopy shading of solar radiation.

[48] While T_d approximates T_s well for daily averages, we note that there are a few caveats. First, we note that errors are more variable for hourly values than for daily averages (Figure 5), and that none of the standard temperatures capture the daily extremes in T_s (Figure 4 and Table 2). This will impact different applications, and the user must consider whether accuracy in hourly T_s values is a priority for their particular application. Differences between T_s and T_d were largest at midday, especially at sites that experienced increased radiative heating (Figure 8). This suggests that the vapor pressure of air at standard height is not in equilibrium with vapor pressure at the snow surface during sunny conditions, signifying a potential increase in the magnitude of latent heat flux at midday, likely due to sublimation. Future work should investigate how to improve upon these findings, such that the maxima and minima in T_s are captured. Second, we assume that there is no vapor pressure gradient when T_s is assumed equal to T_d (i.e., $e_{air} - e_{surf} = 0$). Because radiation dominates the snowmelt energy balance in many climates, we do not expect this to be a major limitation for many applications. However, in settings where latent heat exchange is important, we caution the use of this simple approximation. Finally, we note that instrument uncertainties may be large (based on manufacturer's specified accuracy, Table 1) when measuring T_s, and our analysis assumed that T_s was measured accurately with the infrared sensors and pyrgeometers. Midday observations of T_s were typically within $\pm 1°C$ of the melting point during the melt season, which suggests that the accuracy of the sensors may be better than their specifications, a result also found by *Van den Broeke et al*. [2004]. Likewise, we did not find a substantial relationship between sensor type and T_s representation across the sites (e.g., Figure 8). Using paired sensors at BOG, we found reasonable correspondence between paired infrared sensor measurements and pyrgeometer measurements (supporting information 2). Thus, instrument type did not significantly impact our results, but we recommend more research in how instrument type and differences in field-of-view might influence interpretation of T_s. Sites that measure the energy balance rarely have both types of sensors, and it would be helpful to have more paired measurements to better understand uncertainties in measured T_s.

[49] This study highlights the value in having improved temperature and humidity information in snow-dominant regions and provides strong motivation for expanded monitoring and improved understanding of humidity variations. This adds to the recent results of *Marks et al*. [2013], who found that the timing of $T_d = 0°C$ matched the measured timing of the precipitation phase transition (rain versus snow) better than $T_w = 0°C$ and $T_a = 0°C$ during a winter storm in the Owyhee Mountains (Idaho, USA). Understanding spatial and temporal variations in both air temperature and humidity may, therefore, yield improved representation of both T_s and event-scale precipitation phase across a watershed. However, to realize these benefits fully, it is imperative that operational agencies (e.g., NRCS in the US) expand the number of humidity-observing stations and ensure reliable data quality (i.e., regular calibration of sensors to correct humidity drift). Coordination between snow and wildfire monitoring agencies could also increase the number of humidity observations during the winter (some wildfire weather stations are inactive during the winter) without adding new infrastructure. While humidity measurements are more common than T_s measurements by a factor of 17 in the western US, they are sparse relative to measurements of air temperature [*Raleigh*, 2013], which is a less robust predictor of T_s. Improved understanding of humidity variations between permanent stations might also be accomplished through short-term field campaigns with inexpensive sensors, which have compared reasonably well to NOAA weather stations [see *Feld et al*., 2013 and associated supplement], and numerical weather models. The calibration of hygrometers can significantly impact their reliability, and thus care must be taken to ensure robust calibration is routinely applied [*Ingleby et al*., 2013].

[50] Improved spatial and temporal information of T_d would benefit a number of applications with remote sensing related to T_s. For evaluation purposes, remotely sensed land surface temperature from satellite-based sensors such as MODIS [*Wan and Li*, 1997] or VIIRS [*Guillevic et al*., 2012] could be compared to spatial estimates of T_d in snow-covered environments, particularly at night when T_d reasonably approximates T_s at many locations (Figure 5). The proposed methodology may help to extend understanding of spatial variations of T_s, a key scale issue when using sparse point station measurements to evaluate remotely sensed land surface temperature data sets [*Wang*, 2005; *Hall et al*., 2008]. For the coarse resolution remote sensing products (e.g., MODIS 1 km T_s), pixels with mixed land covers (i.e., snow, forest, bare soil, shade) yield high uncertainty in T_s, enhancing the difficulty of evaluating against surface station observations; understanding of T_d variations around the site may provide useful context in these comparisons. Areas with more homogenous terrain (e.g., the Arctic and cold prairies) may be less prone to this mixed pixel problem and would permit more ideal testing of remote sensing with T_d. Spatial distributions of T_d might also be used to downscale remotely sensed T_s from coarse spatial scales (e.g., $10^1 - 10^3$ m) to finer scales (e.g., $10^0 - 10^1$ m). It was beyond the scope of this study to compare remotely sensed land surface temperature to distributed T_d fields, though the question of spatial variability of these fields is important. Future work should investigate these potential remote sensing applications.

[51] Distributed snow model applications may also benefit from the presented analysis. Snow models are typically evaluated against point observations of SWE and streamflow, which help to assess the representation of the mass balance. However, these variables do not directly reflect variations in the surface energy balance throughout the year, as SWE may only be sensitive to energy bias during

periods of snowmelt [*Wayand et al*., 2013]. Ideally, more weather stations in snow-dominated environments would measure the complete energy balance to better understand errors in modeled processes, but financial and practical considerations preclude this possibility. Distributed hydrology and snow models must estimate shortwave and longwave radiation, and common methods for estimating radiation may have large biases (e.g., 10–100 W m^{-2}) [*Jepsen et al*., 2012] that are undetectable due to a lack of ground measurements. In the absence of such measurements, the method presented here for approximating T_s with minimal data may be useful for model testing because T_s responds directly to variations and bias in the energy balance, and T_d tracks these variations in a similar manner (Figure 9). By using observations of T_d, SWE, runoff, and SCA to evaluate a snow model, the energy and mass balances are considered more holistically. Finally, while we illustrated how T_d might serve as a tool for detecting energy balance bias, we suggest that T_d might alternatively be used as a reasonable prognostic representation of daily T_s for estimating outgoing longwave radiation in distributed radiation snow models, which have often assumed T_s is equivalent to the minimum of T_a and 0°C [e.g., *Molotch*, 2009]. An unresolved issue for this final application is that T_d tends to underestimate T_s as T_s approaches the melting point at some sites (Figure 2). More research is needed to assess how the T_s information embedded in the saturation temperatures (T_d and T_w) may be best applied in numerical models.

[52] **Acknowledgments.** M. Raleigh was supported by a graduate fellowship from the Hydro Research Foundation and a postdoctoral fellowship at the National Center for Atmospheric Research. Additional funding was provided by the National Science Foundation (grant EAR-0838166). The authors thank the UW Mountain Hydrology research group for internal review. The authors acknowledge Danny Marks, Jeff Dozier, one anonymous reviewer, and the WRR editorial staff for providing critical reviews which improved the paper. Field data collection at the OPB, SPY, and BOG sites were funded by the Canadian Foundation for Climate and Atmospheric Science (IP3 Network and DRI Network), the Natural Sciences and Engineering Research Council of Canada, and the Environment Canada Science Horizons Program. Additional funding for the OPB and SPY sites was provided by the Biogeoscience Institute (University of Calgary) and Alberta Ingenuity. Additional funding for the BOG site was provided by the Canadian Space Agency (C-SET Network) and the Government of the Northwest Territories. The authors graciously acknowledge Samuel Morin and CNRM-GAME/CEN for the provision of meteorological and snow data at Col de Porte. The authors would also like to express appreciation to Lindamae Peck, John Fiori, Doug Punt, and the Cold Regions Research and Engineering Laboratory (CREEL) in Hanover, NH for the use of data from the South Royalton (SRV) field site from the SOROIDS project. CRREL is part of the U.S. Army Engineering Research and Development Center (ERDC).

References

Alduchov, O., and R. Eskridge (1996), Improved Magnus form approximation of saturation vapor pressure, *J. Appl. Meteorol.*, *35*, 601–609, doi:10.1175/1520-0450(1996)035<0601:IMFAOS>2.0.CO;2.

Anderson, S. P., and M. F. Baumgartner (1998), Radiative heating errors in naturally ventilated air temperature measurements made from buoys, *J. Atmos. Oceanic Technol.*, *15*(1), 157–173, doi:10.1175/1520-0426(1998)015<0157:RHEINV>2.0.CO;2.

Andreas, E. L. (1986), A new method of measuring the snow-surface temperature, *Cold Reg. Sci. Technol.*, *12*(2), 139–156, doi:10.1016/0165-232X(86)90029-7.

Andreas, E. L. (2002), Parameterizing scalar transfer over snow and ice: A review, *J. Hydrometeorol.*, *3*(4), 417–432, doi:10.1175/1525-7541(2002)003<0417:PSTOSA>2.0.CO;2.

Andreas, E., P. Guest, P. Persson, C. Fairall, T. Horst, R. Moritz, and S. Semmer (2002), Near-surface water vapor over polar sea ice is always near ice saturation, *J. Geophys. Res.*, *107*(C10), 8033, doi:10.1029/2000JC000411.

Arck, M., and D. Scherer (2001), A physically based method for correcting temperature data measured by naturally ventilated sensors over snow, *J. Glaciol.*, *47*(159), 665–670, doi:10.3189/172756501781831774.

Armstrong, R. L., and B. R. Armstrong (1987), Snow and avalanche climates of the western United States: A comparison of maritime, intermountain and continental conditions, *Proceedings of the Davos Symposium on Avalanche Formation, Movement and Effects*, pp. 281–294, IAHS Publ., Davos, Switzerland.

Bales, R. C., N. P. Molotch, T. H. Painter, M. D. Dettinger, R. Rice, and J. Dozier (2006), Mountain hydrology of the western United States, *Water Resour. Res.*, *42*, W08432, doi:10.1029/2005WR004387.

Birkeland, K. W. (1998), Terminology and predominant processes associated with the formation of weak layers of near-surface faceted crystals in the mountain snowpack, *Arct. Alp. Res.*, *30*(2), 193–199, doi:10.2307/1552134.

Birkeland, K. W., R. F. Johnson, and D. S. Schmidt (1998), Near-surface faceted crystals formed by diurnal recrystallization: A case study of weak layer formation in the mountain snowpack and its contribution to snow avalanches, *Arct. Alp. Res.*, *30*(2), 200–204, doi:10.2307/1552135.

Boone, A., and P. Etchevers (2001), An intercomparison of three snow schemes of varying complexity coupled to the same land surface model: Local-scale evaluation at an alpine site, *J. Hydrometeorol.*, *2*, 374–394.

Brubaker, K., A. Rango, and W. Kustas (1996), Incorporating radiation inputs into the snowmelt runoff model, *Hydrol. Processes*, *10*(10), 1329–1343, doi:10.1002/(SICI)1099-1085(199610)10:10<1329::AID-HYP464>3.0.CO;2-W.

Brun, E., E. Martin, V. Simon, C. Gendre, and C. Coleou (1989), An energy and mass model of snow cover suitable for operational avalanche forecasting, *J. Glaciol.*, *35*(121), 333–342.

Clark, M. P., H. K. McMillan, D. B. G. Collins, D. Kavetski, and R. A. Woods (2011), Hydrological field data from a modeller's perspective: Part 2: Process-based evaluation of model hypotheses, *Hydrol. Processes*, *25*(4), 523–543, doi:10.1002/hyp.7902.

Colbeck, S. (1988), The kinetic friction of snow, *J. Glaciol.*, *34*(116), 78–86.

Dozier, J., and T. H. Painter (2004), Multispectral and hypersepctral remote sensing of alpine snow properties, *Annu. Rev. Earth Planet. Sci.*, *32*(1), 465–494, doi:10.1146/annurev.earth.32.101802.120404.

Duguay, C. (1993), Radiation modeling in mountainous terrain review and status, *Mt. Res. Dev.*, *13*(4), 339–357.

Ellis, C. R., J. W. Pomeroy, T. Brown, and J. MacDonald (2010), Simulation of snow accumulation and melt in needleleaf forest environments, *Hydrol. Earth Syst. Sci.*, *14*(6), 925–940, doi:10.5194/hess-14-925-2010.

Essery, R., and P. Etchevers (2004), Parameter sensitivity in simulations of snowmelt, *J. Geophys. Res.*, *109*, D20111, doi:10.1029/2004JD005036.

Essery, R., S. Morin, Y. Lejeune, and C. B. Ménard (2013), A comparison of 1701 snow models using observations from an alpine site, *Adv. Water Resour.*, *55*, 131–148, doi:10.1016/j.advwatres.2012.07.013.

Etchevers, P., et al. (2004), Validation of the energy budget of an alpine snowpack simulated by several snow models (SnowMIP project), *Ann. Glaciol.*, *38*(1), 150–158, doi:10.3189/172756404781814825.

Feld, S. I., N. C. Cristea, and J. D. Lundquist (2013), Representing atmospheric moisture content along mountain slopes: Examination using distributed sensors in the Sierra Nevada, California, *Water Resour. Res.*, *49*, 4424–4441, doi:10.1002/wrcr.20318.

Flanner, M. G., and C. S. Zender (2006), Linking snowpack microphysics and albedo evolution, *J. Geophys. Res.*, *111*, D12208, doi:10.1029/2005JD006834.

Flerchinger, G. N., W. Xaio, D. Marks, T. J. Sauer, and Q. Yu (2009), Comparison of algorithms for incoming atmospheric long-wave radiation, *Water Resour. Res.*, *45*, W03423, doi:10.1029/2008WR007394.

Georges, C., and G. Kaser (2002), Ventilated and unventilated air temperature measurements for glacier-climate studies on a tropical high mountain site, *J. Geophys. Res.*, *107*(D24), 4775, doi:10.1029/2002JD002503.

Guillevic, P. C., J. L. Privette, B. Coudert, M. A. Palecki, J. Demarty, C. Ottlé, and J. A. Augustine (2012), Land surface temperature product validation using NOAA's surface climate observation networks—Scaling methodology for the visible infrared imager radiometer suite (VIIRS), *Remote Sens. Environ.*, *124*, 282–298, doi:10.1016/j.rse.2012.05.004.

Halberstam, I., and J. P. Schieldge (1981), Anomalous behavior of the atmospheric surface layer over a melting snowpack, *J. Appl. Meteorol.*,

20(3), 255–265, doi:10.1175/1520-0450(1981)020<0255:ABOTAS>2.0.CO;2.

Hall, D., J. Box, K. Casey, S. Hook, C. Shuman, and K. Steffen (2008), Comparison of satellite-derived and in-situ observations of ice and snow surface temperatures over Greenland, *Remote Sens. Environ.*, *112*(10), 3739–3749, doi:10.1016/j.rse.2008.05.007.

Helgason, W., and J. Pomeroy (2012), Problems closing the energy balance over a homogeneous snow cover during midwinter, *J. Hydrometeorol.*, *13*(2), 557–572, doi:10.1175/JHM-D-11-0135.1.

Hood, J. L., and M. Hayashi (2010), Assessing the application of a laser rangefinder for determining snow depth in inaccessible alpine terrain, *Hydrol. Earth Syst. Sci.*, *14*(6), 901–910, doi:10.5194/hess-14-901-2010.

Huwald, H., C. W. Higgins, M.-O. Boldi, E. Bou-Zeid, M. Lehning, and M. B. Parlange (2009), Albedo effect on radiative errors in air temperature measurements, *Water Resour. Res.*, *45*, W08431, doi:10.1029/2008WR007600.

Ingleby, B., D. Moore, C. Sloan, and R. Dunn (2013), Evolution and accuracy of surface humidity reports, *J. Atmos. Oceanic Technol.*, *30*(9), 2025–2043, doi:10.1175/JTECH-D-12-00232.1.

Iqbal, M. (1983), *An Introduction to Solar Radiation*, Academic, New York.

Iribarne, J., and W. Godson (1981), *Atmospheric Thermodynamics*, 2nd ed., D. Reidel, Dordrecht, Netherlands.

Jepsen, S. M., N. P. Molotch, M. W. Williams, K. E. Rittger, and J. O. Sickman (2012), Interannual variability of snowmelt in the Sierra Nevada and Rocky Mountains, United States: Examples from two alpine watersheds, *Water Resour. Res.*, *48*, W02529, doi:10.1029/2011WR011006.

Jordan, R. (1991), *A one-dimensional temperature model for a snow cover: Technical documentation for SNTHERM.89, Spec. Rep. 91-16*, p. *58*, U.S. Army Cold Reg. Res. Eng. Lab., Hanover, N. H.

Kent, E. C., R. J. Tiddy, and P. K. Taylor (1993), Correction of marine air temperature observations for solar radiation effects, *J. Atmos. Oceanic Technol.*, *10*(6), 900–906, doi:10.1175/1520-0426(1993)010<0900:COMATO>2.0.CO;2.

Kondo, J., and T. Yamazaki (1990), A prediction model for snowmelt, snow surface temperature and freezing depth using a heat balance method, *J. Appl. Meteorol.*, *29*(5), 375–384, doi:10.1175/1520-0450(1990)029<0375:APMFSS>2.0.CO;2.

Kondo, J., and H. Yamazawa (1986), Measurement of snow surface emissivity, *Boundary Layer Meteorol.*, *34*(4), 415–416, doi:10.1007/BF00120992.

Legates, D. R., and C. J. Willmott (1990), Mean seasonal and spatial variability in global surface air temperature, *Theor. Appl. Climatol.*, *41*(1–2), 11–21, doi:10.1007/BF00866198.

Liston, G. E., and K. Elder (2006), A Meteorological distribution system for high-resolution terrestrial modeling (MicroMet), *J. Hydrometeorol.*, *7*(2), 217–234, doi:10.1175/JHM486.1.

Mahrt, L., and D. Vickers (2005), Boundary-layer adjustment over small-scale changes of surface heat flux, *Boundary Layer Meteorol.*, *116*(2), 313–330, doi:10.1007/s10546-004-1669-z.

Marks, D., J. Dozier, and R. E. Davis (1992), Climate and energy exchange at the snow surface in the alpine region of the Sierra Nevada: 1. Meteorological measurements and monitoring, *Water Resour. Res.*, *28*(11), 3029–3042, doi:10.1029/92WR01482.

Marks, D., J. Kimball, D. Tingey, and T. Link (1998), The sensitivity of snowmelt processes to climate conditions and forest cover during rain-on-snow: A case study of the 1996 Pacific Northwest flood, *Hydrol. Processes*, *12*(10–11), 1569–1587, doi:10.1002/(SICI)1099-1085(199808/09)12:10/11<1569::AID-HYP682>3.0.CO;2-L.

Marks, D., A. Winstral, M. Reba, J. Pomeroy, and M. Kumar (2013), An evaluation of methods for determining during-storm precipitation phase and the rain/snow transition elevation at the surface in a mountain basin, *Adv. Water Resour.*, *55*, 98–110, doi:10.1016/j.advwatres.2012.11.012.

Marsh, P., and J. W. Pomeroy (1996), Meltwater fluxes at an Arctic forest-tundra site, *Hydrol. Processes*, *10*(10), 1383–1400, doi:10.1002/(SICI)1099-1085(199610)10:10<1383::AID-HYP468>3.0.CO;2-W.

Mauder, M., R. L. Desjardins, Z. Gao, and R. van Haarlem (2008), Errors of naturally ventilated air temperature measurements in a spatial observation network, *J. Atmos. Oceanic Technol.*, *25*(11), 2145–2151, doi:10.1175/2008JTECHA1046.1.

Mohammed, G. A., M. Hayashi, C. R. Farrow, and Y. Takano (2013), Improved characterization of frozen soil processes in the versatile soil moisture budget model, *Can. J. Soil Sci.*, *93*(4), 511–531, doi:10.4141/cjss2012-005.

Molotch, N. P. (2009), Reconstructing snow water equivalent in the Rio Grande headwaters using remotely sensed snow cover data and a spatially distributed snowmelt model, *Hydrol. Processes*, *23*(7), 1076–1089, doi:10.1002/hyp.7206.

Morin, S., Y. Lejeune, B. Lesaffre, J.-M. Panel, D. Poncet, P. David, and M. Sudul (2012), An 18-yr long (1993–2011) snow and meteorological dataset from a mid-altitude mountain site (Col de Porte, France, 1325 m alt.) for driving and evaluating snowpack models, *Earth Syst. Sci. Data*, *4*(1), 13–21, doi:10.5194/essd-4-13-2012.

Murray, F. W. (1967), On the computation of saturation vapor pressure, *J. Appl. Meteorol.*, *6*(1), 203–204, doi:10.1175/1520-0450(1967)006<0203:OTCOSV>2.0.CO;2.

Musselman, K. N., N. P. Molotch, S. A. Margulis, P. B. Kirchner, and R. C. Bales (2012), Influence of canopy structure and direct beam solar irradiance on snowmelt rates in a mixed conifer forest, *Agric. For. Meteorol.*, *161*, 46–56, doi:10.1016/j.agrformet.2012.03.011.

Nakamura, R., and L. Mahrt (2005), Air temperature measurement errors in naturally ventilated radiation shields, *J. Atmos. Oceanic Technol.*, *22*(7), 1046–1058, doi:10.1175/JTECH1762.1.

Outcalt, S. I. (1972), The development and application of a simple digital surface-climate simulator, *J. Appl. Meteorol.*, *11*(4), 629–636, doi:10.1175/1520-0450(1972)011<0629:TDAAOA>2.0.CO;2.

Outcalt, S. I., C. Goodwin, G. Weller, and J. Brown (1975), Computer simulation of the snowmelt and soil thermal regime at Barrow, Alaska, *Water Resour. Res.*, *11*(5), 709–715, doi:10.1029/WR011i005p00709.

Painter, T. H., A. P. Barrett, C. C. Landry, J. C. Neff, M. P. Cassidy, C. R. Lawrence, K. E. McBride, and G. L. Farmer (2007), Impact of disturbed desert soils on duration of mountain snow cover, *Geophys. Res. Lett.*, *34*, L12502, doi:10.1029/2007GL030284.

Peck, L. (1994), *Variation in visual and near-infrared contrast with a snow background, Spec. Rep. 94-28*, p. *27*, U.S. Army Cold Reg. Res. Eng. Lab, Hanover, NH.

Peck, L., and J. Fiori (1992), *Soil Temperatures at South Royalton, Vermont, USA*, Natl. Snow Ice Data Cent., Boulder, Colo. [Available at http://nsidc.org/data/ggd489.html.]

Peterson, E. W., and J. P. Hennessey (1978), On the use of power laws for estimates of wind power potential, *J. Appl. Meteorol.*, *17*(3), 390–394, doi:10.1175/1520-0450(1978)017<0390:OTUOPL>2.0.CO;2.

Pohl, S., P. Marsh, and G. E. Liston (2006), Spatial-temporal variability in turbulent fluxes during spring snowmelt, *Arct. Antarct. Alp. Res.*, *38*(1), 136–146, doi:10.1657/1523-0430(2006)038[0136:SVITFD]2.0.CO;2.

Pomeroy, J. W., D. M. Gray, K. R. Shook, B. Toth, R. L. H. Essery, A. Pietroniro, and N. Hedstrom (1998), An evaluation of snow accumulation and ablation processes for land surface modelling, *Hydrol. Processes*, *12*(15), 2339–2367, doi:10.1002/(SICI)1099-1085(199812)12:15<2339::AID-HYP800>3.0.CO;2-L.

Raleigh, M. S. (2013), Quantification of Uncertainties in Snow Accumulation, Snowmelt, and Snow Disapperance Dates, PhD thesis, 206 pp., Dept. of Civil and Env. Eng., Univ. of Wash., Seattle, Wash.

Shea, C., and B. Jamieson (2011), Some fundamentals of handheld snow surface thermography, *Cryosphere*, *5*(1), 55–66, doi:10.5194/tc-5–55-2011.

Singh, V., and D. Frevert (Eds.) (2002), *Mathematical Models of Small Watershed Hydrology and Applications*, Water Resour. Publ., Highlands Ranch, Colo.

Slater, A. G., et al. (2001), The representation of snow in land surface schemes: Results from PILPS 2(d), *J. Hydrometeorol.*, *2*(1), 7–25, doi:10.1175/1525–7541(2001)002<0007:TROSIL>2.0.CO;2.

Stössel, F., M. Guala, C. Fierz, C. Manes, and M. Lehning (2010), Micrometeorological and morphological observations of surface hoar dynamics on a mountain snow cover, *Water Resour. Res.*, *46*, W04511, doi:10.1029/2009WR008198.

Tarboton, D., and C. Luce (1996), *Utah Energy Balance Snow Accumulation and Melt Model (UEB), Computer Model Technical Description Users Guide*, p. *64*, Utah Water Res. Lab., USDA For. Serv. Intermt. Res. Stn, Logan, UT.

U.S. Army Corps of Engineers (1956), Snow hydrology, summary report of the snow investigations, p. 437, U.S. Army Corps of Engineers, North Pac. Div., Portland, Ore.

Van den Broeke, M., D. van As, C. Reijmer, and R. van de Wal (2004), Assessing and improving the quality of unattended radiation observations in Antarctica, *J. Atmos. Oceanic Technol.*, *21*(9), 1417–1431, doi:10.1175/1520-0426(2004)021<1417:AAITQO>2.0.CO;2.

Wagner, W., and J. Horel (2011), Observations and simulations of snow surface temperature on cross-country ski racing courses, *Cold Reg. Sci. Technol.*, *66*(1), 1–11, doi:10.1016/j.coldregions.2010.12.003.

Wan, Z., and Z. Li (1997), A physics-based algorithm for retrieving land-surface emissivity and temperature from EOS/MODIS data, *IEEE Trans. Geosci. Remote Sens.*, *35*(4), 980–996, doi:10.1109/36.602541.

Wang, K. (2005), Estimation of surface long wave radiation and broadband emissivity using moderate resolution imaging spectroradiometer (MODIS) land surface temperature/emissivity products, *J. Geophys. Res.*, *110*, D11109, doi:10.1029/2004JD005566.

Watson, F. G. R., W. B. Newman, J. C. Coughlan, and R. A. Garrott (2006), Testing a distributed snowpack simulation model against spatial observations, *J. Hydrol.*, *328*(3–4), 453–466, doi:10.1016/j.jhydrol.2005.12.012.

Wayand, N. E., A. F. Hamlet, M. Hughes, S. I. Feld, and J. D. Lundquist (2013), Intercomparison of meteorological forcing data from empirical and mesoscale model sources in the N.F. American River Basin in northern Sierra Nevada, California, *J. Hydrometeorol.*, *14*(3), 677–699, doi:10.1175/JHM-D-12-0102.1.

Whiteman, C. (2000), *Mountain Meteorology: Fundamentals and Applications*, Oxford Univ. Press, New York.

Wigmosta, M. S., L. W. Vail, and D. P. Lettenmaier (1994), A distributed hydrology-vegetation model for complex terrain, *Water Resour. Res.*, *30*, 1665–1679, doi:10.1029/94WR00436.

Williams, T. J., W. L. Quinton, and J. L. Baltzer (2013), Linear disturbances on discontinuous permafrost: Implications for thaw-induced changes to land cover and drainage patterns, *Environ. Res. Lett.*, *8*(2), 025006, doi:10.1088/1748-9326/8/2/025006.